Bulk and surface magnetoinductive breathers in binary metamaterials

M. I. Molina,[1] N. Lazarides,[2,3] and G. P. Tsironis[2,3]

[1]*Departamento de Física, Facultad de Ciencias, Universidad de Chile, Casilla 653, Santiago, Chile*
[2]*Department of Physics, University of Crete, P.O. Box 2208, 71003 Heraklion, Greece*
[3]*Institute of Electronic Structure and Laser, Foundation for Research and Technology-Hellas, P.O. Box 2208, 71003 Heraklion, Greece*

We investigate theoretically the existence of bulk and surface discrete breathers in a one-dimensional magnetic metamaterial comprised of a periodic binary array of split-ring resonators; the two types of resonators used have different resonant frequencies caused by unequal slit sizes. We use the rotating-wave approximation and construct several types of breather excitations both for the energy-conserving as well as dissipative-driven case; we corroborate these approximate results trough numerically exact computations. We demonstrate that discrete breathers can appear spontaneously in the dissipative-driven system as a result of a fundamental instability.

I. INTRODUCTION

Discrete breathers (DBs) or intrinsic localized modes, are time-periodic and spatially localized excitations that may be produced generically in discrete arrays of weakly coupled nonlinear elements [1,2]. A large body of theoretical work has produced means of precise numerical analysis of coupled oscillator systems with breathers both in the Hamiltonian as well as dissipative regimes [3–7]. Breathers have been experimentally observed in several diverse systems, including optical waveguides [8], solid-state systems [9,10], antiferromagnetic chains [11], Josephson-junction arrays [12], and micromechanical oscillators [13,14]. Discrete breathers can be generated spontaneously in a lattice either through stochastic [15,16] or by purely deterministic mechanisms [17–20] in a process by which energy, initially evenly distributed in a nonlinear lattice, can be localized into large amplitude nonlinear excitations. Indeed, it has been demonstrated experimentally [13,20] that the standard modulational instability (MI) mechanism in dissipative systems driven by an alternating term can initiate that process through the formation of low-amplitude breathers. The energy exchange between low-amplitude DBs favors the higher-amplitude ones, resulting eventually in the formation of a few high-amplitude DBs.

Recently, a new class of artificially structured materials, referred to as metamaterials, was discovered; the latter is comprised of discrete elements and exhibit electromagnetic properties not available in naturally occurring materials. A subclass of those metamaterials, the magnetic metamaterials (MMs), exhibit significant magnetic properties and negative magnetic response up to terahertz (THz) and optical frequencies [21,22]. The most common realization of a MM is composed of periodically arranged electrically small subwavelength particles, referred to as split-ring resonators (SRRs) [23,24]. In its simplest form, each of the resonators is a highly conducting metallic ring with a slit. The MM thus built can become nonlinear either by the insertion of a nonlinear dielectric [25] or by connecting a nonlinear electronic component (e.g., a varactor diode) [26,27] across the gap of each SRR, resulting in voltage-dependent SRR capacitance.

In microwave frequencies, such a MM has been realized [28] and is dynamically tunable by varying the input power. In a metamaterial where discreteness and nonlinearity are present, excitations of the type of discrete breather may form. Recent work in one and two-dimensional metamaterial lattices has shown existence and stability of DBs in nonlinear SRR-based MM models; the latter my be localized either in the bulk [29,30] or at the surface [31] of the MM. Additionally, domain walls [32] as well as envelope solitons [33] may be excited in these systems. We note that surface DBs in MMs are similar to surface modes observed in discrete waveguide arrays [34,35].

The focus of the present work is in binary MMs constituted of two types of nonlinear SRRs, each with different electrical properties, that interact inductively and form a one-dimensional (1D) lattice. We investigate units with cubic nonlinearity, although the results do not change qualitatively for other types of nonlinearity. A binary nonlinear SRR lattice may lead to the observation of phase-matched parametric interaction and enhanced second-harmonic generation [36]. In practice, a binary MM can be constructed in many different ways, by changing for example one or more of the material and/or the geometrical parameters of the SRRs belonging to one type (say type *a*), with respect to the same parameters of the SRRs belonging to the other type (say type *b*). Here we allow for different slit widths in the two SRRs leading to resonance frequency mismatch (RFM). The considered binary MM is formed by type *a* SRRs at the even-numbered sites and type *b* SRRs at the odd-numbered sites of a periodic 1D array. In the next section we give the model equations that describe the dynamics of the binary MM and we obtain the corresponding linear dispersion relation for magnetoinductive waves in that medium [37,38]. In Secs. III and IV we use the rotating-wave approximation (RWA) and construct several types of Hamiltonian as well as dissipative breathers (DDBs). The linear stability of the DBs is discussed in Sec. V where the full model equations are integrated numerically. In most of the investigated cases the numerics confirm the quality of the RWA results. We also demonstrate the possibility of spontaneous generation of DDBs induced through MI by using frequency chirping of the driving field. This is the same procedure used for the

FIG. 1. (Color online) One-dimensional binary array of split-ring resonators.

experimental generation of high-amplitude DDBs in micromechanical cantilever oscillator arrays [13] and thus may be also used in experiments involving nonlinear binary MMs. Finally, in Sec. VI we conclude.

II. MODEL BINARY METAMATERIAL AND LINEAR DISPERSION

Consider a 1D SRR-based MM comprised of nonlinear units shown schematically in Fig. 1. Each nonlinear SRR in the array can be mapped to a nonlinear resistor-inductor-capacitor (RLC) circuit featuring self-inductance L, Ohmic resistance R, and nonlinear (voltage-dependent) capacitance $C(|\mathbf{E}|^2) \propto \epsilon(|\mathbf{E}_g|^2)$, where ϵ is the field-dependent permittivity of the infilling dielectric, $\mathbf{E}$ is the electric field, and $\mathbf{E}_g$ is the electric field induced along the SRR slit. We assume that the latter originates from an alternating magnetic field that is applied to the MM perpendicularly to the SRR planes, and it is proportional to the voltage U across the slit.

Let us for the moment ignore the nonlinearity and set $C = C_l$, with C_l is the linear capacitance that is built up across the slit. Just like an RLC resonator, the SRRs exhibit an inductive-capacitive resonance at frequency $\omega_R \simeq 1/\sqrt{LC_l}$ (for $R \simeq 0$, implying low Ohmic losses). For a circular SRR with circular cross section, the parameters L, R, and C_l of the equivalent RLC circuit can be estimated from the relations [21]

$$L = \mu_0 r\left[\log\left(\frac{16r}{h}\right) - 1.75\right], \quad C_l = \epsilon_0 \epsilon_l \frac{\pi h^2}{4d}, \quad R = \frac{8\rho r}{h^2} \tag{1}$$

where ϵ_0 and μ_0 are the permittivity and permeability in vacuum, respectively, ϵ_l is the linear relative dielectric permittivity of the infilling dielectric, r is the average SRR radius, h is the diameter of the metal wire, d is the slit width of the SRR, and ρ the (material-dependent) SRR resistivity. Neighboring SRRs in an array are magnetically coupled through their mutual inductance M, which is approximately given by

$$M \approx \frac{\mu_0 \pi r_a^2 r_b^2}{4D^3} \tag{2}$$

where D is their center-to-center distance, and r_a, r_b are their average radii. In order to construct a binary array, we have to change one or more of the material and/or geometrical parameters of the SRRs that are going to be of one type, with respect to the same parameters of the SRRs that are going to be of the other type. As it can be observed from Eqs. (1) and (2):

(i) a change in the SRR radius r affects L, M, and R;
(ii) a change in h affects L, C_l, and R;

(iii) a change in ϵ_l affects C_l which in turn, implies a change in the nonlinear response;
(iv) a change in d affects C_l and slightly R and L; and
(v) A change in resistivity ρ affects R.

Obviously there many possibilities for constructing two types of SRRs and consequently a binary array. Here we make the relatively simple choice to create two types of SRRs by considering different slit widths, i.e., d_a for type a and d_b for type b. Thus, the linear capacitances of type a and b SRRs become respectively C_a and C_b, resulting in different resonance frequencies $\omega_a = 1/\sqrt{LC_a}$ and $\omega_b = 1/\sqrt{LC_b}$.

Now let us return to the nonlinear problem, and assume that the slits of all the SRRs in the array are filled with a Kerr-type dielectric. Then, the charge Q_n accumulated in the capacitor of the nth SRR is [39]

$$Q_n = C_n\left(1 + \chi\frac{U_n^2}{U_c^2}\right)U_n \tag{3}$$

where $C_n = C_a$ ($C_n = C_b$) for SRRs at even- (odd-)numbered sites of the array, and $\chi = \alpha/(3\epsilon_l)$ is the dimensionless nonlinearity coefficient, with $\alpha = +1$ ($\alpha = -1$) for a self-focusing (self-defocusing) dielectric. The above equation leads to the following approximate form for the voltage U_n across the slit of the nth SRR,

$$U_n \approx \frac{Q_n}{C_n}\left[1 - \chi\frac{1}{U_c^2}\left(\frac{Q_n}{C_n}\right)^2\right] \tag{4}$$

where U_c is a characteristic (large) voltage. Then, the coupled equations describing the charge dynamics in the nonlinear MM that is placed in an alternating magnetic field are generally written as

$$\frac{d^2}{dt^2}[MQ_{2n-1} + L_{2n}Q_{2n} + MQ_{2n+1}] + R_{2n}\frac{d}{dt}Q_{2n} + \frac{1}{C_{2n}}Q_{2n}$$
$$- \chi\frac{1}{U_c^2}\left(\frac{Q_{2n}}{C_{2n}}\right)^3 = F(t) \tag{5}$$

$$\frac{d^2}{dt^2}[MQ_{2n} + L_{2n+1}Q_{2n+1} + MQ_{2n+2}]$$
$$+ R_{2n+1}\frac{d}{dt}Q_{2n+1}\frac{1}{C_{2n+1}}Q_{2n+1} - \chi\frac{1}{U_c^2}\left(\frac{Q_{2n+1}}{C_{2n+1}}\right)^3 = F(t), \tag{6}$$

where we assume that $R_m = R$, $L_m = L$, and

$$F(t) = \mathcal{E}_0 \sin(\omega t). \tag{7}$$

The above equation gives the electromotive force (emf) of amplitude $\mathcal{E}_0$ and frequency ω that is excited in each SRR due to the action of the field. Let us define the quantities

$$Q_c = \sqrt{C_a C_b}U_c, \quad q_n = Q_n/Q_c,$$

$$\tau = \sqrt{\omega_a \omega_b}t \equiv \omega_0 t, \quad \gamma = R\sqrt{\frac{\sqrt{C_a C_b}}{L}}. \tag{8}$$

With the above definitions, Eqs. (5) and (6) can be written in normalized form as

$$\frac{d^2}{d\tau^2}[\lambda q_{2n-1} + q_{2n} + \lambda q_{2n+1}] + \delta q_{2n} - \chi\delta^3 q_{2n}^3$$

$$= -\gamma\frac{dq_{2n}}{d\tau} + \epsilon_0 \sin(\Omega\tau), \tag{9}$$

$$\frac{d^2}{d\tau^2}[\lambda q_{2n} + q_{2n+1} + \lambda q_{2n+2}] + \frac{q_{2n+1}}{\delta} - \chi\frac{q_{2n+1}^3}{\delta^3}$$

$$= -\gamma\frac{dq_{2n+1}}{d\tau} + \epsilon_0 \sin(\Omega\tau), \tag{10}$$

where $\lambda \equiv M/L$ is the dimensionless coupling parameter, $\Omega = \omega/\omega_0$ is the dimensionless driving frequency, $\delta \equiv \omega_a/\omega_b$ is the RFM ratio, $\epsilon_0 = \mathcal{E}_0/U_c$, and n is an integer. From Eqs. (9) and (10) we can see that the change in the linear capacitances also affects the nonlinear terms, and that, actually, the latter are affected much more than the linear ones. The changes that are caused to the terms proportional to R and L are of higher order and thus they are neglected. As the RFM δ increases, the resonance frequency as well as the nonlinear term of the even-numbered site SRRs increase, while at the same time the resonance frequency and the nonlinear term of the odd-numbered site SRRs decrease. The inductive coupling parameter λ can be either positive or negative depending on whether the array geometry is of the "axial" or "planar" type [30].

Such MMs and other systems with magnetically coupled elements, support in the low-amplitude (linear) limit a new kind of waves, the magnetoinductive waves [37,38]. In the present case, the frequency dispersion for linear magnetoinductive waves is obtained by substituting

$$q_{2n} = ae^{i(2n\kappa - \Omega\tau)}, \quad q_{2n+1} = be^{i((2n+1)\kappa - \Omega\tau)}, \tag{11}$$

where κ is the normalized wavenumber, into linearized Eqs. (9) and (10), without the dissipative and the external driving terms ($\gamma = 0$ and $\epsilon_0 = 0$),

$$\Omega_\pm^2 = \frac{[\delta + (1/\delta)] \pm \sqrt{[\delta + (1/\delta)]^2 - 4(1 - 4\lambda^2 \cos^2 \kappa)}}{2(1 - 4\lambda^2 \cos^2 \kappa)}. \tag{12}$$

The dispersion curves for a particular choice of RFM δ and coupling parameter λ are shown in Fig. 2. Even though we can think of each linear SRR as an RLC circuit, i.e., an electromagnetic oscillator, we notice that the dispersion curves for the coupled array do not contain any acousticlike branch; rather both curves are of the "optical" type: $\lim_{k\to 0} \Omega(k) \neq 0$. This is due to the particular (inductive) nature of the coupling between the SRRs. There are now three regions where we can look for breathers in the nonlinear case: Above and below the bands, and in the Bragg gap (BG) in between. In the absence of RFM ($\delta = 1$) we recover the single band for the "monoatomic" MM [30]. As δ diverges from unity the BG increases, pushing the Ω_+ branch upwards and the Ω_- branch downwards.

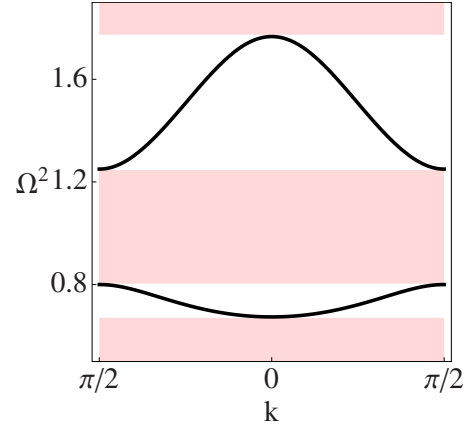Equations (9) and (10) can be written conveniently in the compact form,

FIG. 2. (Color online) Linear dispersion relation for the binary SRR array, for $\delta = 0.8$ and $\lambda = -0.2$.

$$\frac{d^2}{d\tau^2}[\lambda q_{n-1} + q_n + \lambda q_{n+1}] + \omega_n^2 q_n - \chi\omega_n^6 q_n^3$$

$$= -\gamma\frac{dq_n}{d\tau} + \epsilon_0 \sin(\Omega\tau), \tag{13}$$

where $\omega_n^2 = \delta$ ($\omega_n^2 = 1/\delta$) for even (odd) n. Without dissipation and external driving, Eq. (13) can be obtained from the Hamiltonian $\mathcal{H} = \Sigma_n \mathcal{H}_n$, where the discrete Hamiltonian density $\mathcal{H}_n$ is given by

$$\mathcal{H}_n = \frac{1}{2}\{\dot{q}_n^2 + \lambda\dot{q}_n(\dot{q}_{n-1} + \dot{q}_{n+1})\} + V_n. \tag{14}$$

The last term on the right-hand side of the earlier equation is the nonlinear on-site potential which is given by

$$V_n \equiv V(q_n) = \frac{1}{2}(\omega_n q_n)^2\left[1 - \frac{1}{2}\chi\omega_n^2(\omega_n q_n)^2\right]. \tag{15}$$

The Hamiltonian $\mathcal{H}$ is actually the conserved energy of the lossless system in the absence of any driving terms system. For the dissipative system, $\mathcal{H}$ is also useful since its time-average per period gives correctly the average energy per period for that system.

III. HAMILTONIAN BREATHERS IN THE ROTATING-WAVE APPROXIMATION

A standard method of DB construction in Hamiltonian systems, that gives numerically exact results up to arbitrary precision, uses the Newton's method [4,5], which has been applied successfully for DB generation in MMs [29,30]. In this Section, we use the RWA method that keeps a simple physical picture and moreover can produce quite accurate results. According to the simplest version of that method, one looks for stationary solutions of the system that are separable with an assumed time dependence (e.g., sinusoidal) of the form $q_n(\tau) = q_n \sin(\Omega\tau)$. Direct substitution of $q_n(\tau)$ into Eq. (13) with the approximation $\sin(x)^3 \approx (3/4)\sin(x)$ gives an algebraic system of nonlinear equations for the q_ns that reads as
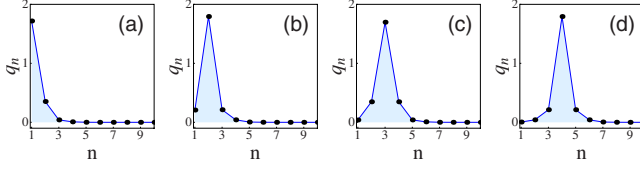
FIG. 3. (Color online) Typical Hamiltonian surface breather profiles centered at (a) surface, (b) one layer away from surface, (c) two layers away from surface, and (d) three layers away from surface in a magnetoinductive binary chain for $\delta = 0.9$, $\lambda = 0.1$, $\Omega = 0.77$, and $\chi = 1/6$ obtained by the RWA.

$$-\Omega^2(\lambda q_{n+1} + q_n + \lambda q_{n-1}) + \omega_n^2 q_n - (3/4)\chi\omega_n^6 q_n^3 = 0. \tag{16}$$

In the anticontinuous limit ($\lambda \to 0$) the earlier equation has solutions

$$q_n = 0 \quad \text{or} \quad q_n^2 = \frac{\omega_n^2 - \Omega^2}{(3/4)\chi\omega_n^6}. \tag{17}$$

According to Eq. (17), we have the following interesting possible scenarios:

(i) $\chi > 0$. Then, $q_n^2 > 0$ for all n, if $\Omega^2 < \text{Min}\{\delta, 1/\delta\}$;

(ii) $\chi < 0$. Then $q_n^2 > 0$ for all n provided $\Omega^2 > \text{Max}\{\delta, 1/\delta\}$; and

(iii) in the intermediate case where $\text{Min}\{\delta, 1/\delta\} < \Omega^2 < \text{Max}\{\delta, 1/\delta\}$, what happens is that $q_{2n} > 0$ and $q_{2n+1} = 0$, or the converse, depending upon the sign of α.

The RWA method can be used for the construction of DBs both on the "surface" and the bulk of the energy-conserved binary MM. For a 1D MM, a surface-localized DB obviously corresponds to an edge state, i.e., a state with maximum amplitude at either of the two ends of the array. A bulk DB, on the other hand, is meant to be a DB whose maximum amplitude is far from the endpoints of the array. However, the procedure of obtaining DBs by the RWA method, both at the surface or in the bulk, proceeds in the same way. The first step is to set up a trivial DB. We first choose its central site, i.e., the site where the DB shall have its maximum amplitude. Suppose that the central site is taken at $n = n_B$ where the "coordinate" $q_n = q_{n_B}$ and set all the q_n for $n \neq n_B$ equal to zero. The value of q_{n_B} is calculated from Eq. (17), with an appropriately chosen Ω. That solution is subsequently continued for finite couplings up to a maximum value $\lambda = \lambda_{\max}$ where DBs cease to exist. Usually we consider a DB to be localized around the site where it exhibits its maximum amplitude. For a finite array, the boundary conditions that should be imposed to the dynamic equations resulting from Hamiltonian (14) should be specified. For DBs excited in the bulk one may use either periodic or open-ended boundary conditions, since DBs are highly localized entities and are not affected by the boundaries. However, for surface DBs the termination of the structure should be taken into account, and for that purpose we should use open-ended boundary conditions. In the following, we always use that type of boundary conditions, i.e., $q_0 = 0$, $q_{N+1} = 0$, where N is the total number of SRRs in the binary array.

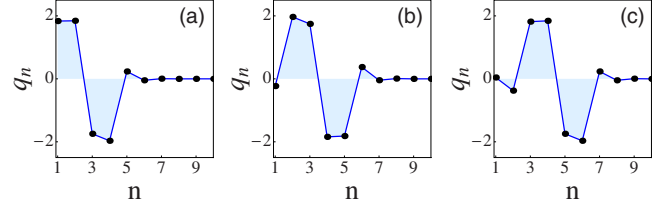*Surface breathers.* Typical surface-localized single-site

FIG. 4. (Color online) Typical Hamiltonian surface multisite breather profiles in a magnetoinductive binary chain for $\delta = 0.9$, $\lambda = -0.1$, $\Omega^2 = 0.77$, and $\chi = 1/6$ obtained by the RWA.

DBs that are generally very similar to the ones examined for a discrete nonlinear Schrödinger model for a semi-infinite binary waveguide array [40], are displayed in Fig. 3. The unstaggered modes shown there originate in the lower gap region $0 < \Omega < \text{Min}[\delta, 1/\delta]$. There are also staggered modes (not shown) originating from the Bragg gap region that constitute magnetoinductive Tamm states [30,31]. From the surface DBs shown in Fig. 3, only one of them [Fig. 3(a)] corresponds to a truly surface state, since it is localized exactly at the left end of the array ($n = 1$). The next two [Figs. 3(b) and 3(c)] can also be characterized as surface DBs since they are localized very close to the surface ($n = 2$ and $n = 3$, respectively), but actually they are crossover states between surface and bulk DBs. Since the DBs shown here are highly localized, they obtain their bulk form within a distance of only a few sites from the surface, so that the DB shown in Fig. 3(d) (localized at $n = 4$) can be considered as a bulk DB. With the appropriate choice of the initial conditions we may also construct multisite surface DBs such as those shown in Fig. 4 that remind four-site antisymmetric DB excitations. Of course, close to the surface, we cannot obtain exact antisymmetric DBs.

Bulk breathers. Typical bulk Hamiltonian DB profiles obtained with the RWA method are shown in Figs. 5 and 6. In Fig. 5, the two single-site symmetric DBs differ in that the first one [Fig. 5(a)] is staggered, while the other one [Fig. 5(b)] is unstaggered. The staggered/unstaggered character of those Hamiltonian DBs depends on the sign of the product of the coupling parameter and the nonlinearity parameter, $\sigma = \text{sgn}(\alpha\lambda)$. For $\sigma > 0$, which implies either $\alpha = +1$ and $\lambda > 0$ or $\alpha = -1$ and $\lambda < 0$, the excited DBs are unstaggered. On the other hand, for $\sigma < 0$, that implies either $\alpha = +1$ and $\lambda < 0$ or $\alpha = -1$ and $\lambda > 0$, the excited DBs are staggered. In that figure the DB frequency $\Omega_B = 2\pi/T_B$, with T_B the DB period,
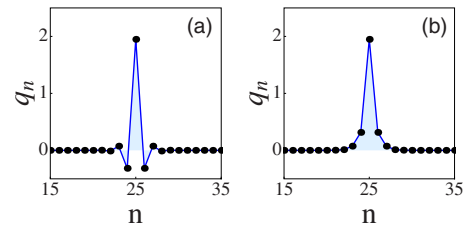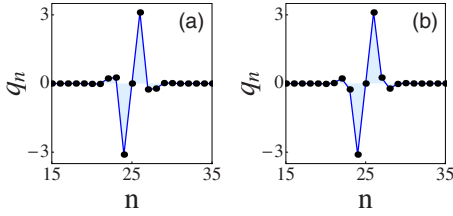

FIG. 5. (Color online) Typical Hamiltonian bulk symmetric breather profiles in a magnetoinductive binary chain for $\delta = 0.8$, $\chi = -1/6$, $\Omega^2 = 1.5$, and (a) Staggered mode with $\lambda = +0.1$; (b) unstaggered mode with $\lambda = -0.1$. These profiles are also obtained by the RWA.

FIG. 6. (Color online) Typical Hamiltonian bulk antisymmetric breather profiles in a magnetoinductive binary chain for $\delta=0.5$, $\chi=-1/6$, $\Omega^2=0.8$, and (a) $\lambda=-0.2$; (b) $\lambda=+0.2$. These profiles are also obtained by the RWA.

was chosen to ensure that the DB amplitude at all sites is nonzero in the anticontinuous limit. In Fig. 6, that shows two-site antisymmetric bulk DBs, the nonlinearity parameter is negative ($\alpha=-1$) and $\mathrm{Min}[\delta,1/\delta]<\Omega^2<\mathrm{Max}[\delta,1/\delta]$, implying that in the anticontinuous limit, only the even sites of the array can have a nonzero amplitude. Again, with appropriate choice of the initial conditions and by changing the sign of the coupling parameter λ and/or the nonlinearity parameter α we may also construct multisite bulk DBs with different symmetry. It should be also possible to generate a large variety of surface and bulk Hamiltonian DBs in two-dimensional binary arrays, just like in planar arrays of identical SRRs [30]. Increased dimensionality offers more possibilities for generating different DB types.

IV. DISSIPATIVE BREATHERS IN THE ROTATING-WAVE APPROXIMATION

We consider now the more realistic case of DDBs that can be excited either on the "surface" or the bulk of a 1D binary MM. In typical experiments that involve MMs, the metamaterial is driven by an applied electromagnetic field of appropriate polarization. In 1D there are two possible geometries for the arrangement of the SRRs [30]; the planar geometry (as shown in Fig. 1), for which the coupling parameter is negative, and the axial geometry for which the coupling parameter is positive. That polarization can be chosen such that, for example, the magnetic component of the field is perpendicular to the SRR planes, while there is no electric-field component across the SRR gap. This choice simplifies physically the situation since only the magnetic field excites an emf in the SRRs. Thus, in the equivalent circuit picture, a binary SRR-based MM in an electromagnetic field can be described by an array of nonlinear RLC circuits driven by an alternating emf that are coupled through their mutual inductances. The losses of the SRRs can be described in this picture by an equivalent resistance. That effective resistance R may actually describe both Ohmic losses of the SRR as well as radiative losses, if these are relatively low [33]. Under those assumptions, the dynamics of the charges $q_n(\tau)$, $n=1,2,\ldots,N$, is given by Eq. (13). In the framework of the RWA method, we look for stationary solutions of that equation in the form $q_n(\tau)=q_n\sin(\Omega\tau+\phi_n)$. By direct substitution of $q_n(\tau)$ into Eq. (13) and by making the RWA replacement $\sin(\Omega\tau+\phi_n)^3\approx(3/4)\sin(\Omega\tau+\phi_n)$, where q_n thereafter denotes the time-independent DB amplitude at the nth site and
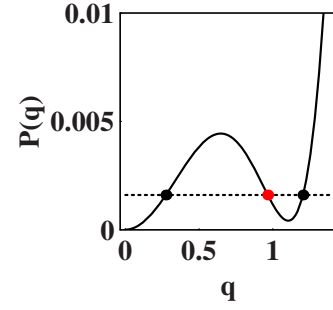

FIG. 7. (Color online) The intersection of $P(q_n)$ (solid line) and ε_0^2 (dashed line) provides the nonlinear attractor(s) for a single SRR. Case displayed here corresponds to $\delta=1$, $\chi=1/6$, $\gamma=0.02$, $\Omega=0.92$, $\epsilon_0=0.04$. The black [gray (red online)] circle represents a stable (unstable) attractor.

ϕ_n its phase, we find that the DB amplitudes and phases at each site n satisfy the relations

$$\left[-\Omega^2(\lambda q_{n+1}+q_n+\lambda q_{n-1})+\omega_n^2 q_n-\frac{3}{4}\chi\omega_n^6 q_n^3\right]^2+\gamma^2\Omega^2 q_n^2=\epsilon_0^2$$

(18)

$$\phi_n=\tan^{-1}\left[\frac{-\gamma\Omega q_n}{\omega_n^2 q_n-\Omega^2(\lambda q_{n+1}+q_n+\lambda q_{n-1})-\frac{3\chi}{4}\omega_n^6 q_n^3}\right]$$

(19)

where $n=1,2,\ldots,N$ and $q_0=q_{N+1}=0$. The inclusion of dissipation and external driving alters significantly the possible DB modes that the binary SRR system can support. The dissipative DBs possess the character of an attractor for initial conditions in the corresponding basin of attraction, and they may appear as a result of power balance between the incoming power and the intrinsic power loss [6,7]. Dissipative DB excitations in SRR-based MMs are of great importance since they alter locally the magnetic response of the system from diamagnetic to paramagnetic or vice versa [29–31].

In the anticontinuous limit Eqs. (18) and (19) become

$$P(q_n)\equiv q_n^2\left\{\left[\omega_n^2-\Omega^2-\frac{3}{4}\chi\omega_n^6 q_n^2\right]^2+\gamma^2\Omega^2\right\}=\varepsilon_0^2, \quad (20)$$

$$\phi_n=\tan^{-1}\left[\frac{-\gamma\Omega}{(\omega_n^2-\Omega^2)-\frac{3}{4}\chi\omega_n^6 q_n^2}\right], \quad (21)$$

where we kept the subscript n to distinguish between oscillators located either at an odd-numbered site ($n=$odd integer) or even-numbered site ($n=$even integer). The polynomial $P(q_n)$ is cubic in q_n^2 for general values of the parameters δ, χ, Ω, and γ, with $P(0)=0$.

Thus, there can be at most three real roots that correspond to attractors of the SRR oscillator (see Fig. 7) from which two are stable and one is unstable. However, by varying a parameter in that four-dimensional parameter space, two of these solutions may disappear through a pitchfork bifurca-
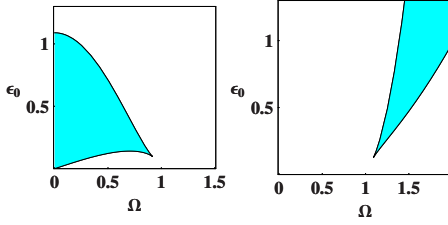
FIG. 8. (Color online) "Phase diagram" in the reduced parameter space $\epsilon_0 - \Omega$ for a single driven-damped SRR oscillator showing the regions with different number of attractors, for $\delta=1$, $\gamma=0.1$, and $\chi=+1/6$ (left); $\chi=-1/6$ (right). Inside (outside) the colored region we have three (one) attractors.

FIG. 10. (Color online) Dissipative surface breather profiles for $\delta=2$, $\Omega=0.5$, $\lambda=0.025$, $\chi=+1/6$, $\gamma=0.01$, and $\epsilon_0=0.04$, which are localized at (a) $n=1$, (b) $n=2$, and (c) $n=3$.

tion, leaving behind only a single attractor. The boundary in parameter space that separates those two cases can be found implicitly by computing the values of q_n denoted by q_n^*, for which $dP(q_n)/dq_n=0$ [i.e., the values of q_n that correspond to the local extrema of $P(q_n)$]. Clearly, if $q_n=q_n^*$ corresponds to a local minimum (maximum) then for $P(q_n^*)<\epsilon_0^2$ [$P(q_n^*)>\epsilon_0^2$] there is only one attractor left. Thus, the earlier inequalities determine different regions in the parameter space where, depending on the values of the parameters, we may have either one or three attractors. Thus, we may distinguish in such a diagram two different "phases" that correspond to either three or one real solutions. A typical example is shown in the reduced $\epsilon_0 - \Omega$ parameter space in Fig. 8, for $\delta=1$ (no RFM) and opposite values of χ, while the values of the driving field strength ϵ_0 and the driving frequency Ω are varying. There we see clearly the areas where there are either three (inside colored area) or one (outside colored area) attractor(s). Another example, where the RFM changes from $\delta=0.5-1.5$ is shown in Fig. 9 for $\gamma=0.1$ and positive χ. There we observe that the colored area, corresponding to three attractors, expands with increasing δ. The values for the stable attractors predicted by the RWA are in excellent agreement with those obtained through dynamical evolution of the charge in a single SRR oscillator. For instance, for the parameter set $\delta=0.8$, $\Omega=0.92$, $\gamma=0.01$, $\epsilon_0=0.04$, $\chi=+1/6$, and for an even-numbered site n, Eq. (20) predicts a single attractor at $q_1^e=\pm 0.582\,163$, while for an odd-numbered site it predicts three attractors at $q_1^o=\pm 1.235\,31$, $q_2^o=\pm 1.330\,55$ and $q_3^o=\pm 0.099\,681\,1$, of which the latter two are stable. The unstable attractor at q_1^o is not reachable through simple numerical integration of the dynamical equation. For the stable attractors, we have checked with direct numerical integration that their values are practically the same with those obtained from the RWA approach. In general, the presence of
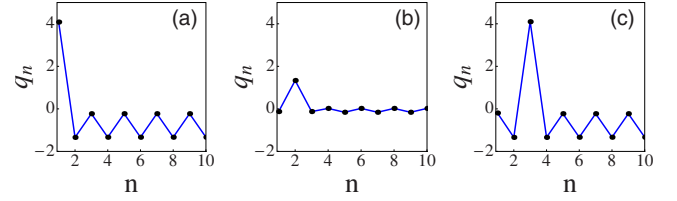
dissipation and driving severely limit the possible spatial profile of the breathers. The structures tend now to be either strongly localized ones, or rather extended, like domain walls [27,29]. The situation is similar for DDBs in the bulk (Figs. 10 and 11). As soon as δ deviates from unity, that is, when we are dealing with a *bona fide* binary chain, the area in phase space with two stable attractors reduce (increase) as δ decreases (increases) from unity, if the site chosen is an even-numbered one, as can be seen in Fig. 9. The opposite behavior occurs for an odd-numbered site.

In order to illustrate how the RWA method works in this case, we calculate some of typical surface DDBs. The calculation of bulk DDBs proceeds in the same way, by simply choosing the central site of the corresponding trivial DB that is located at $n=n_B$ somewhere in the bulk. For a given value of the RFM, we first determine the attractors available for each single SRR oscillator located either at odd- or even-numbered site. Then, we set up a trivial surface DB which is subsequently continued for finite values of λ. The continuation procedure proceeds in exactly the same way as that for Hamiltonian DBs except that the relevant equations are now Eqs. (18) and (19). We thus can obtain several types of surface DDBs for an interval of λ up to a maximum, i.e., up to $\lambda=\lambda_{max}$. For example, for the parameter set $\chi=+1/6$, $\gamma=0.01$, $\Omega=0.5$, $\delta=2$, and $\epsilon_0=0.04$, we have stable attractors $q_1^o=\pm 4.067\,19$ and $q_2^o=\pm 0.160\,225$ at odd-numbered sites, and $q_1^e=\pm 1.334$ and $q=\pm 0.022\,863\,9$ at even-numbered sites. We can set up a trivial surface DB localized at $n_B=1$ as $q_1=4.067\,19$, $q_{2n}=0.022\,863\,9$ and $q_{2n-1}=0.160\,225$ ($n>1$). For a trivial surface DB localized at $n_B=2$ we may choose $q_2=1.334$. $q_{2n-1}=-0.160\,225$ and $q_{2n}=-0.022\,863\,9$ ($n>1$). Or, for a trivial surface DB localized at $n_B=3$ we may choose $q_{2n}=-0.160\,225$, $q_{2n-1}=-0.160\,225$ ($n\neq 2$), and $q_3=4.067\,19$. Continuation of those trivial DDBs up to $\lambda=0.025$ gives the surface DDB profiles shown in Fig. 10. Of course there also other trivial DDB profiles that we could choose. Similar bulk DDBs can be obtained from the trivial
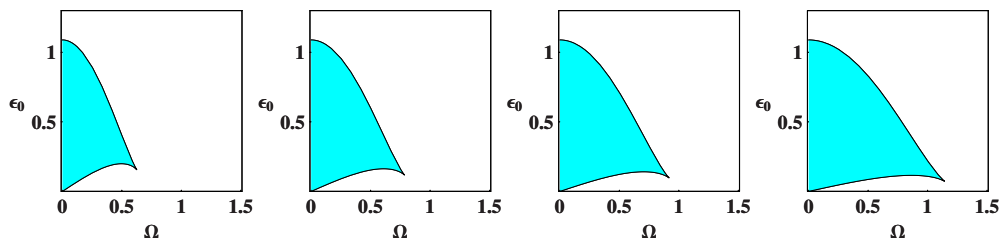

FIG. 9. (Color online) Same as in Fig. 8 for a single driven-damped SRR oscillator with $\gamma=0.1$, $\chi=+1/6$, and (from left to right) $\delta=0.5$; $\delta=0.75$; $\delta=1$; and $\delta=1.5$.
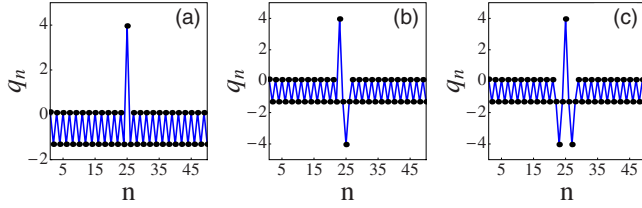
FIG. 11. (Color online) (a) Single-site, (b) two-site, and (c) three-site dissipative bulk breather profiles localized at odd-numbered sites for $\delta=2$, $\Omega=0.5$, $\lambda=0.025$, $\chi=+1/6$, $\gamma=0.01$, and $\epsilon_0=0.04$.

DDBs given above only by changing n_B to a value relatively far from the endpoints. An illustrative example of a bulk DDB localized at an odd-numbered site is shown on Fig. 11(a), while Figs. 11(b) and 11(c) show multisite DDBs also localized at odd-numbered sites. The latter two DDBs have been obtained with an appropriate choice of a trivial DDB profile.

V. NUMERICALLY EXACT CALCULATIONS

In this section we construct several types of both energy-conserved and dissipative DBs, which are localized either in the bulk or at the surface, using standard numerical algorithms [4,5]. Moreover, in the case of a dissipative binary MM we also generate DDB excitations through a procedure that can be used for parameter values where the homogeneous solution is modulationally unstable [13]. In other words, we exploit MI to initiate spontaneous localization of energy in the binary array [17].

Hamiltonian breathers. For the Hamiltonian binary MM, DBs can be constructed from the anticontinuous limit of Eq. (13) with $\epsilon_0=0$ and $\gamma=0$ where all the SRRs are decoupled [29,30]. Using Newton's method we have constructed several types of Hamiltonian, numerically exact DBs for the 1D binary MM, for different parameter sets. The obtained Hamiltonian DB profiles are in excellent agreement with those obtained with the RWA method.

Dissipative Breathers. In order to generate DDBs we start from the anticontinuous limit of Eq. (13), where dissipation and driving are included. We identify stable attractors of each SRR oscillator, that is either located at odd- or even-numbered sites. For constructing a trivial DDB profile we need to find, for at least one of the two types of oscillators, two different amplitude stable attractors. For example, for the parameter set $\delta=2.0$, $\Omega=0.5$, $\gamma=0.01$, $\epsilon_0=0.04$, and $\chi=+1/6$, we obtain stable attractors $q_1^o=\pm 4.067\,19$ and $q_2^o=\pm 0.160\,225$ at odd-numbered sites, and $q_1^e=\pm 1.334$ and $q^e=\pm 0.022\,863\,9$ at even-numbered sites. Those values are practically the same with those obtained with the RWA method. We set up a trivial surface DB localized at $n_B=1$ as $q_1=4.067\,19$, $q_{2n}=0.022\,863\,9$, and $q_{2n-1}=0.160\,225$ ($n>1$). For a trivial surface DB localized at $n_B=3$ we may choose $q_3=4.067\,19$, $q_{2n}=0.022\,863\,9$, and $q_{2n-1}=-0.160\,225$ ($n\neq 2$). Continuation of those trivial DDBs gives surface DDB profiles up to $\lambda_{max}\simeq 0.19$. Typical profiles for several values of λ, both for DDBs localized at $n=1$ and $n=3$, are shown in Fig. 12.
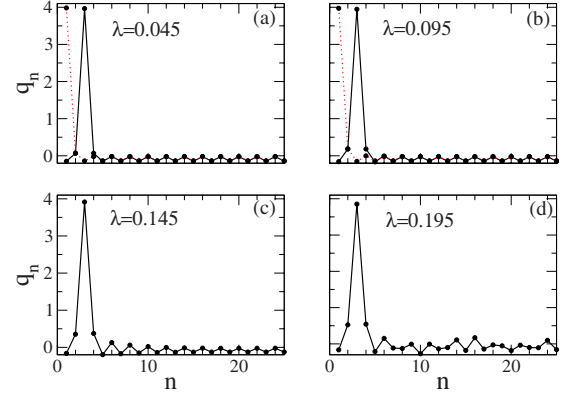

FIG. 12. (Color online) Dissipative breather profiles at maximum amplitude for several values of the coupling parameter as shown on the figure which are localized at $n=1$ and $n=3$. The parameters are $\Omega=0.5$, $\chi=+1/6$, $\gamma=0.01$, $\epsilon_0=0.04$, and $\delta=2$.

Another example is given for the parameter set $\delta=0.8$, $\Omega=0.92$, $\gamma=0.01$, $\varepsilon_0=0.04$, and $\chi=+1/6$, where the RWA method predicts a single attractor at $q_1^e=\pm 0.582163$ at even-numbered site oscillators, while it predicts three attractors at $q_1^o=\pm 1.235\,31$, $q_2^o=\pm 1.330\,55$, and $q_3^o=\pm 0.099\,681\,1$, of which the latter two are stable, for an odd-numbered site oscillators. These values are also in agreement with those obtained by direct integration of the single SRR oscillators. We set up a trivial surface DDB localized at $n_B=1$ as $q_1=1.330\,55$, $q_{2n}=0.582\,163$, and $q_{2n-1}=0.099\,681\,1$ ($n>1$), and continue it up to $\lambda_{max}\sim 0.07$ where DDBs cease to exist. Typical DDB profiles are shown in Fig. 13 for several values of λ shown on the figure. A profile for $\lambda=0.072$ which is greater that λ_{max}, where the homogeneous solution is restored, is also shown in Fig. 13. The frequency of the DDBs shown here is the same with that of the driver, i.e., $\Omega_B \equiv 2\pi/T_B=\Omega$. However, the phase differences of the SRR oscillators in the array with respect to the driving field are generally different for each oscillator, as can be observed in Fig. 14, where the time evolution of q_1-q_4 is followed for
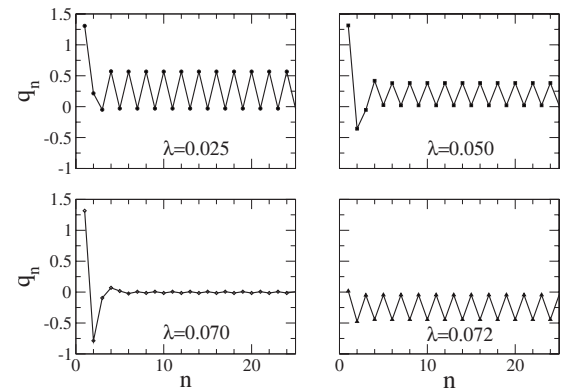

FIG. 13. Dissipative breather profiles at maximum amplitude for several values of the coupling parameter as shown on the figure which are localized at the surface (at $n=1$), along with an almost uniform solution for $\lambda=0.072$ just above the value of λ_{max} for this particular parameter set. The parameters are $\Omega=0.92$, $\chi=+1/6$, $\gamma=0.01$, $\epsilon_0=0.04$, and $\delta=0.8$.
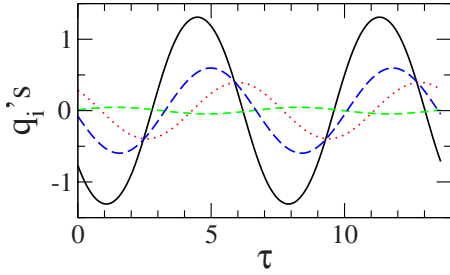
FIG. 14. (Color online) Time dependence of q_1 (black solid curve), q_2 (red dotted curves), q_3 (green short-dashed curve), and q_4 (blue dashed curves), for a surface breather localized at $n=1$ and $\lambda=0.03$. The other parameters are the same with those in the caption of Fig. 13.

approximately two periods T_B of the DDB oscillation. Note also that even though the time evolution seems practically sinusoidal (harmonic), that may not be necessarily true for DDBs obtained with some other parameter set.

Dissipative breathers by frequency chirping. For a frequency gapped linear spectrum, some of the linear modes become unstable at large amplitude. If the curvature of the dispersion curve in the region of that mode is negative and the lattice potential is hard then, the large amplitude mode becomes unstable with respect to formation of a DB in the gap above the linear spectrum [13,20]. Below we exploit MI in order to generate spontaneously DDBs in the binary array. The procedure that is followed is shortly described below [13,20]. For the parameters in the captions of Figs. 15 and 16, the top of the upper linear band is located at $\Omega \simeq 1.42$ where the curvature is negative. Moreover, the SRRs are subjected to on-site potentials that are hard (for $\chi < 0$). The (large amplitude) driver is initiated with its frequency just below Ω and is then chirped with time to produce enough vibrational amplitude to induce MI of the uniform mode, which then leads to spontaneous DDB generation. At the end of the frequency chirping phase, the driver frequency is well above Ω, and only supplies energy into the formed DDB(s). During that phase, a large number of DDBs may be generated, which can move and collide and eventually coalesce into a small number of high-amplitude DDBs that are frequency locked to the driver and, because of that, they are trapped at particular SRRs. After that, the driver frequency is kept constant and the high-amplitude DDBs (and even some low-amplitude ones) continue to receive energy falling into a
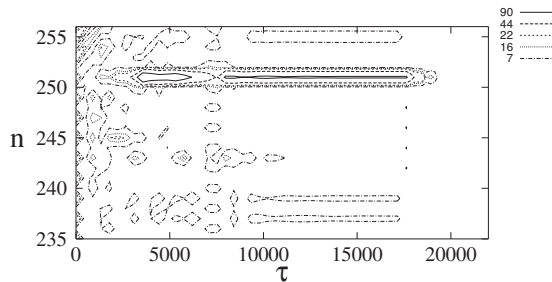

FIG. 15. Contours of the energy density $\mathcal{H}_n$ on the $\tau - n$ plane for a strongly driven binary magnetic metamaterial, with $\delta=2$, $\Omega=1.42$, $\chi=-1/6$, $\gamma=0.001$, $\lambda=0.05$, and $\varepsilon_0=3.0$.

FIG. 16. Contours of the energy density $\mathcal{H}_n$ on the $\tau - n$ plane for a strongly driven binary magnetic metamaterial, with $\delta=2$, $\Omega=1.42$, $\chi=-1/6$, $\gamma=0.001$, $\lambda=0.05$, and $\varepsilon_0=2.0$.
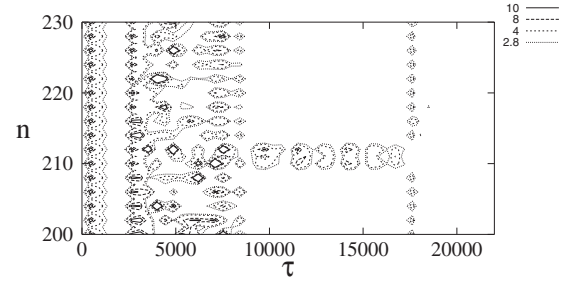
stationary state. When the driver is switched off all DDBs die out in a short-time interval.

In Figs. 15 and 16, the contours of the energy density $\mathcal{H}_n$ on the $\tau - n$ plane identify the evolution of the DDBs formed by that procedure. The chirping phase lasts for $2000T_0$ time units ($T_0=2\pi/\Omega$), where the frequency varies linearly from $\Omega_i=0.997 \; \Omega$ to $\Omega_f=1.020 \; \Omega$. The driver is subsequently kept at constant frequency Ω_f until it is switched off after another $2000 \; T_0$ time units. Figures 15 and 16 correspond to the regions of the binary MMs where several DDBs have survived after the chirping phase. In Fig. 15 we clearly observe a high-amplitude DDB at $n=251$, along with some other DDBs of considerably lower amplitude, that survive until the end of the constant frequency phase. In Fig. 16, where the binary MM is driven not as strongly as that in Fig. 15, we observe one relatively low-amplitude DDB which however survives until the end of the constant frequency phase. It is possible that the procedure described above, which relies on the MI of the large amplitude linear modes, can be used for the generation of DDBs in other magnetoinductive systems as well as [41,42] in their binary versions.

VI. CONCLUSION

We presented detailed analysis for induced nonlinear localization in binary nonlinear magnetic metamaterials. The systems we analyzed are one dimensional and consist of two types of SRRs; this configuration leads to a linearized magnetoinductive system with two optical bands separated by a gap. When nonlinearity is also taken into account nonlinear localized modes of discrete breather type may be generated in the gaps. We focused on both the Hamiltonian as well as the dissipative case; the latter case is the most interesting physically since it corresponds to true propagation of waves in the medium. We used two approaches, one based on the rotating-wave approximation and the other on exact numerics using the breather analysis from the anticontinuous limit. The comparison of the two shows that the RWA is in most cases a good approximation for a relatively accurate breather construction.

In the Hamiltonian case we found two types of breathers with even or odd local symmetry depending on the sign of the product of the coupling parameter and the nonlinearity parameter. Both types may exist in the bulk but also in the boundary of the chain; the latter form surface breathers. A

similar situation occurs also in the dissipative case where depending on the number of attractors of the single driven nonlinear oscillator system we have different type of dissipative breathers. Both bulk and surface breathers appear with corresponding symmetries.

The binary structure of the lattice allows for generation of breathers through direct external induction. This is accomplished through frequency chirping to the desired frequency. In the process of frequency modulation induction, plane-wave instability occurs that leads to breather generation.

These induced breathers move around in the lattice, collide, some decay and eventually a single breather of much larger size is left in the metamaterial. This method of breather generation is direct and may be used for experimental breather investigation in metamaterials.

[1] A. J. Sievers and S. Takeno, Phys. Rev. Lett. **61**, 970 (1988).

[2] For a recent review see S. Flach and A. V. Gorbach, Phys. Rep. **467**, 1 (2008).

[3] R. S. MacKay and S. Aubry, Nonlinearity **7**, 1623 (1994).

[4] S. Aubry, Physica D **103**, 201 (1997).

[5] J. L. Marín and S. Aubry, Nonlinearity **9**, 1501 (1996).

[6] J. L. Marín, F. Falo, P. J. Martínez, and L. M. Floría, Phys. Rev. E **63**, 066603 (2001).

[7] D. Zueco, P. J. Martínez, L. M. Floría, and F. Falo, Phys. Rev. E **71**, 036613 (2005).

[8] H. S. Eisenberg, Y. Silberberg, R. Morandotti, A. R. Boyd, and J. S. Aitchison, Phys. Rev. Lett. **81**, 3383 (1998).

[9] B. I. Swanson, J. A. Brozik, S. P. Love, G. F. Strouse, A. P. Shreve, A. R. Bishop, W.-Z. Wang, and M. I. Salkola, Phys. Rev. Lett. **82**, 3288 (1999).

[10] F. M. Russell and J. C. Eilbeck, EPL **78**, 10004 (2007).

[11] U. T. Schwarz, L. Q. English, and A. J. Sievers, Phys. Rev. Lett. **83**, 223 (1999).

[12] E. Trías, J. J. Mazo, and T. P. Orlando, Phys. Rev. Lett. **84**, 741 (2000).

[13] M. Sato, B. E. Hubbard, A. J. Sievers, B. Ilic, D. A. Czaplewski, and H. G. Craighead, Phys. Rev. Lett. **90**, 044102 (2003).

[14] M. Sato and A. J. Sievers, Phys. Rev. Lett. **98**, 214101 (2007).

[15] G. P. Tsironis and S. Aubry, Phys. Rev. Lett. **77**, 5225 (1996).

[16] K. O. Rasmussen, S. Aubry, A. R. Bishop, and G. P. Tsironis, Eur. Phys. J. B **15**, 169 (2000).

[17] T. Dauxois and M. Peyrard, Phys. Rev. Lett. **70**, 3935 (1993).

[18] D. Hennig, L. Schimansky-Geier, and P. Hänggi, EPL **78**, 20002 (2007).

[19] D. Hennig, S. Fugmann, L. Schimansky-Geier, and P. Hänggi, Acta Phys. Pol. B **39**, 1125 (2008).

[20] M. Sato, B. E. Hubbard, and A. J. Sievers, Rev. Mod. Phys. **78**, 137 (2006).

[21] M. Gorkunov, M. Lapine, E. Shamonina, and K. H. Ringhofer, Eur. Phys. J. B **28**, 263 (2002).

[22] S. Linden, C. Enkrich, G. Dolling, M. W. Klein, J. Zhou, T. Koschny, C. M. Soukoulis, S. Burger, F. Schmidt, and M. Wegener, IEEE J. Sel. Top. Quantum Electron. **12**, 1097 (2006).

[23] T. J. Yen, W. J. Padilla, N. Fang, D. C. Vier, D. R. Smith, J. B. Pendry, D. N. Basov, and X. Zhang, Science **303**, 1494 (2004).

[24] N. Katsarakis, G. Konstantinidis, A. Kostopoulos, R. S. Penciu, T. F. Gundogdu, M. Kafesaki, E. N. Economou, Th. Koschny, and C. M. Soukoulis, Opt. Lett. **30**, 1348 (2005).

[25] T. H. Hand and S. A. Cummer, J. Appl. Phys. **103**, 066105 (2008).

[26] D. A. Powell, I. V. Shadrivov, Yu. S. Kivshar, and M. V. Gorkunov, Appl. Phys. Lett. **91**, 144107 (2007).

[27] I. V. Shadrivov, S. K. Morrison, and Yu. S. Kivshar, Opt. Express **14**, 9344 (2006).

[28] I. V. Shadrivov, A. B. Kozyrev, D. van der Weide, and Yu. S. Kivshar, Appl. Phys. Lett. **93**, 161903 (2008).

[29] N. Lazarides, M. Eleftheriou, and G. P. Tsironis, Phys. Rev. Lett. **97**, 157406 (2006).

[30] M. Eleftheriou, N. Lazarides, and G. P. Tsironis, Phys. Rev. E **77**, 036608 (2008).

[31] N. Lazarides, G. P. Tsironis, and Yu. S. Kivshar, Phys. Rev. E **77**, 065601 (2008); M. Eleftheriou, N. Lazarides, G. P. Tsironis, and Yu. S. Kivshar, Phys. Rev. E **80**, 017601 (2009).

[32] I. V. Shadrivov, A. A. Zharov, N. A. Zharova, and Yu. S. Kivshar, Photonics Nanostruct. Fundam. Appl. **4**, 69 (2006).

[33] I. Kourakis, N. Lazarides, and G. P. Tsironis, Phys. Rev. E **75**, 067601 (2007).

[34] M. I. Molina, R. A. Vicencio, and Yu. S. Kivshar, Opt. Lett. **31**, 1693 (2006).

[35] Yu. S. Kivshar and M. I. Molina, Wave Motion **45**, 59 (2007).

[36] M. V. Gorkunov, I. V. Shadrivov, and Yu. S. Kivshar, Appl. Phys. Lett. **88**, 071912 (2006).

[37] E. Shamonina, V. A. Kalinin, K. H. Ringhofer, and L. Solymar, J. Appl. Phys. **92**, 6252 (2002).

[38] I. V. Shadrivov, A. N. Reznik, and Yu. S. Kivshar, Physica B **394**, 180 (2007).

[39] A. A. Zharov, I. V. Shadrivov, and Y. S. Kivshar, Phys. Rev. Lett. **91**, 037401 (2003).

[40] M. I. Molina, I. L. Garanovich, A. A. Sukhorukov, and Yu. S. Kivshar, Opt. Lett. **31**, 2332 (2006).

[41] N. Lazarides, G. P. Tsironis, and M. Eleftheriou, Nonlinear Phenom. Complex Syst. (Dordrecht, Neth.) **11**, 250 (2008).

[42] G. P. Tsironis, N. Lazarides, and M. Eleftheriou, PIERS Online **5**, 26 (2009).